10-1-2004

DNA Binding Provides a Molecular Strap Activating the Adenovirus Proteinase

Mark R. Chance
Case Western Reserve University, mark.chance@case.edu

Author(s) ORCID Identifier:

Mark R. Chance

Recommended Citation

Sayan Gupta, Walter F. Mangel, William J. McGrath, Jennifer L. Perek, Donna W. Lee, Keiji Takamoto, Mark R. Chance. DNA Binding Provides a Molecular Strap Activating the Adenovirus Proteinase. Molecular & Cellular Proteomics, Volume 3, Issue 10, 2004, Pages 950-959, https://doi.org/10.1074/mcp.M400037-MCP200.

DNA Binding Provides a Molecular Strap Activating the Adenovirus Proteinase*[S]

Sayan Gupta‡, Walter F. Mangel§, William J. McGrath§, Jennifer L. Perek§, Donna W. Lee§, Keiji Takamoto‡, and Mark R. Chance‡¶

Human adenovirus proteinase (AVP) requires two cofactors for maximal activity: pVIc, a peptide derived from the C terminus of adenovirus precursor protein pVI, and the viral DNA. Synchrotron protein footprinting was used to map the solvent accessible cofactor binding sites and to identify conformational changes associated with the binding of cofactors to AVP. The binding of pVIc alone or pVIc and DNA together to AVP triggered significant conformational changes adjacent to the active site cleft sandwiched between the two AVP subdomains. In addition, upon binding of DNA to AVP, it was observed that specific residues on each of the two major subdomains were significantly protected from hydroxyl radicals. Based on the locations of these protected side-chain residues and conserved aromatic and positively charged residues within AVP, a three-dimensional model of DNA binding was constructed. The model indicated that DNA binding can alter the relative orientation of the two AVP domains leading to the partial activation of AVP by DNA. In addition, both pVIc and DNA may independently alter the active site conformation as well as drive it cooperatively to fully activate AVP. ***Molecular & Cellular Proteomics 3:950–959, 2004.***

The human adenovirus serotype 2 proteinase (AVP)[1] is required for the synthesis of infectious virus (1, 2). Biochemical studies with the recombinant form of AVP showed that AVP requires two cofactors for maximal proteinase activity (3–6). One cofactor is the eleven amino acid residue peptide pVIc, originating from the C terminus of the precursor protein pVI. This peptide is covalently linked to AVP through a disulfide bond as well as by charge-charge and hydrogen bonding interactions (7). The second cofactor is the viral DNA. The K_m for protease activity is reduced 10-fold upon binding each cofactor separately. However, a cooperative effect is observed in the presence of both cofactors, resulting in an overall 34,000-fold increase in the macroscopic kinetic constant (k_{cat}/K_m) compared with free AVP (8, 9). AVP is originally synthesized in an inactive, precursor form as fully activated AVP could cleave virion precursor proteins prior to virion assembly preventing virus particle formation. Indeed, if exogenous pVIc is added to cells along with adenovirus, the amount of infectious virus synthesized is severely diminished compared with when no exogenous pVIc is added (6, 10). It may be that during virus particle maturation inactive AVP binds to viral DNA to become partially active. The partially activated enzyme cleaves out the second cofactor (pVIc) from viral precursor protein pVI, which binds to the AVP-DNA complex to activate it further. The fully active ternary complex of enzyme and cofactors then moves along the viral DNA, cleaving other viral precursor proteins to generate infectious virus particles (8, 9).

The location of the pVIc binding site on AVP is known; the mode of DNA binding is unknown. The crystal structure of AVP bound to the pVIc peptide is shown in Fig. 1*a* (7, 11). The structure has two major domains, with the active site sandwiched between the domains. The pVIc cofactor interacts with both domains forming an antiparallel β-sheet with strand 5 of domain 1, while its N terminus interacts with strand 7 from domain 2. Biochemical studies show that DNA binding is not sequence-specific (5); both electrostatic and nonelectrostatic forces are important to binding (8). Fig. 1*b* depicts the surface charge distribution on AVP; positively charged clusters are seen that may be involved in nonspecific DNA binding (10, 11).

This work defines a three-dimensional model of DNA binding to AVP. This was accomplished by using hydroxyl radical mediated protein footprinting to probe the specific interactions of AVP with its cofactors (12, 13). AVP was irradiated with white synchrotron x-ray radiation and reactive surface-exposed amino acid residues became oxidized. The experiment was then repeated but with cofactors bound to AVP. The observation of robust protections located adjacent to conserved, positively charged, and aromatic residues on the AVP surface suggested specific sites that are involved in contacting DNA (12–14). Also, cofactor-induced conformational changes adjacent to the active site are detected indicative of the molecular mechanisms of cofactor-induced protease activation (15–17).

EXPERIMENTAL PROCEDURES

Biochemicals and Synchrotron Exposures—pVIc (GVQSLKRRRCF) was purchased from Research Genetics (Huntsville, AL), and 12-mer

From the ‡Center for Synchrotron Biosciences, Department of Physiology & Biophysics, Albert Einstein College of Medicine, Bronx, NY 10461; and §Department of Biology, Brookhaven National Laboratory, Upton, NY 11973

Received, March 9, 2004, and in revised form, June 23, 2004
Published, MCP Papers in Press, June 24, 2004, DOI 10.1074/mcp.M400037-MCP200

[1] The abbreviations used are: AVP, adenovirus proteinase; ssDNA, single-stranded DNA.

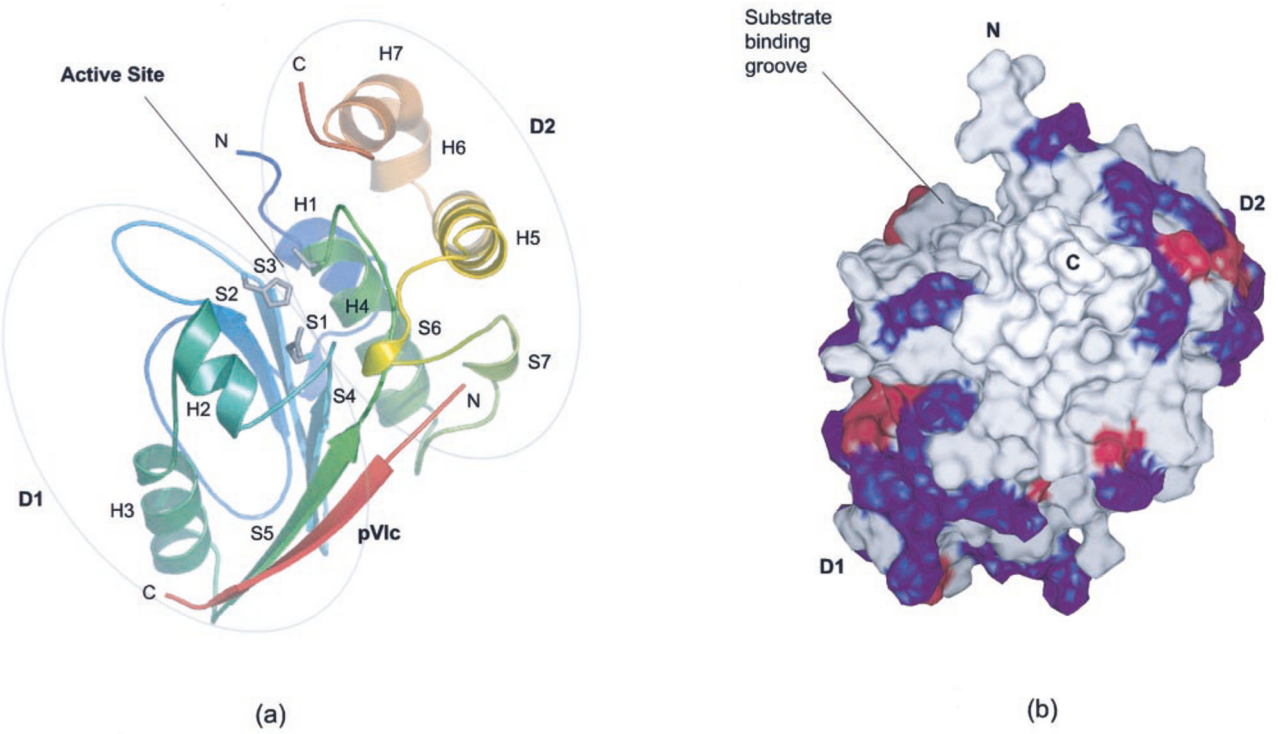

FIG. 1. **Ribbon diagram representation of the AVP-pVIc complex.** *a*, the path of the polypeptide chain of AVP is color-coded according to the visible spectrum with *violet* at the N terminus and *red* at the C terminus. The protein consists of two domains, D1 and D2, indicated by *dotted lines*. D1 consists of sheets S1-S4 and helices H2 and H3 from the N-terminal half of the molecule. D2 is composed of helices H4 to H7 and sheets S6 and S7 from the C-terminal half of the protein, as well as H1, which is from the N terminus. Residues 17–21, which join H1 and S1, and 111–114 from S5, which interacts with S6, provide connections between the two subdomains (7, 11). The pVIc peptide, colored *red*, is at the front of the β-strands in the figure. The positions of the active site residues are shown in stick representation. *b*, a space filling model of the AVP-pVIc complex showing the distribution of basic (*blue*) and acidic (*red*) amino acid residues on the surface.

single-stranded DNA (ssDNA) (GACGACTAGGAT) was purchased from Life Technologies (Rockville, MD). AVP was purified as described previously (5, 18). The concentrations of AVP, pVIc, and DNA were measured as described previously (19, 20). Samples were exposed to white light x-rays from the National Synchrotron Light Source beamline X-28C at the Brookhaven National Laboratory (Upton, NY) as described and then frozen (12, 21–23).

Complex Formation—AVP and its binary complexes with pVIc or with DNA or the tertiary complex of AVP-pVIc-DNA were prepared to a final concentration of 10 μM in 10 mM cacodylate (pH 7.4) and then irradiated with synchrotron radiation for varying time intervals. Complexes with 12-mer ssDNA were formed by incubating 10 μM 12-mer ssDNA with 10 μM AVP. Because the K_d for 12-mer ssDNA and AVP is 63 nM, at 10 μM, virtually all of the 12-mer ssDNA will be bound to AVP (8). The K_d of pVIc for AVP is 4.4 μM (6). To ensure that at 10 μM, all of the pVIc will be bound to AVP, covalent complexes between AVP and pVIc were formed overnight at concentrations of 100 μM each, and the resultant AVP-pVIc covalent complexes diluted to 10 μM. Under the conditions in which the synchrotron footprinting were carried out, the binary complexes and the tertiary complex were fully active enzymatically (data not shown).

Protease Digestion of AVP—Trypsin (Promega, Madison, WI) or chymotrypsin (Roche, Indianapolis, IN) was added to radiolyzed and control protein samples to an enzyme: protein ratio of 1:40 (w/w) in the presence of 10% acetonitrile, 0.2 mM DTT and 0.1 μM $CaCl_2$. The samples were incubated at 37 °C for 12 h. The nine tryptic peptides from the digests of AVP, AVP-pVIc, AVP-DNA, and AVP-pVIc-DNA that have been identified by LC-ESI-MS are shown in Table I. In this table we include only the data for peptides where we have been able to collect high signal-to-noise dose response plots for multiple states of the AVP protein. Similarly, six chymotryptic peptides (16–21, 76–80, 126–129, 134–141, 142–147, and 159–167) were examined (Supplementary Table I); together these peptides cover nearly two-thirds of the sequence of AVP, which contains 204 amino acid residues.

Chromatography and Mass Spectrometry—The digested peptide samples were introduced into the ion source of the mass spectrometer via a Waters Alliance 2690 high pressure LC system (Waters Corp., Milford, MA) as described elsewhere (12, 23). MS data were acquired using a quadrupole ion trap mass spectrometer (ThermoFinnegan LCQ, ThermoFinnegan Inc., San Jose, CA) equipped with an electrospray ion source as previously described (12, 23). The oxidation products were quantitated using the peak intensities of the mass spectral signals. The fraction of peptide modified was determined from the ratio of the intensity under ion signals for the oxidized radiolytic products to the sum of those for the unoxidized peptides and the oxidized radiolytic products (12, 23). The oxidized radiolytic products include +14, +16, +32, and +48 Da species relative to the unmodified ions. The fraction unmodified peptide determined from the average value of duplicate experiments *versus* exposure times (a "dose response" plot) was fit to an exponential decay function with Origin version 6.1 (OriginLabs, Northampton, MA) to determine the rate of peptide modification. The Origin program, using 95% confidence limits of the fitting results, determined the reported errors of the rate data.

Solvent Accessibility Calculations—The solvent accessibilities of individual side chains in the AVP-pVIc were determined from the

TABLE I

Rates of radiolytic modification for the tryptic peptides derived from AVP and its complexes with the cofactors, DNA and pVIc[a]

Peptide and molecular weight		Peptide sequences and accessible surface area values (in Å^2) of selected amino acid side chains[b]	Modified amino acid residue(s) identified by MS/MS[c]	Modification rate (s^{-1})			
				AVP	AVP-DNA	AVP-pVIc	AVP-pVIc-DNA
1–9	1,007.5	**M** G S S E Q E L K 166	(1M)	11.2 ± 1.5	1.0 ± 0.1	–	0.9 ± 0.09
29–37	1,014.5	**F P** G **F** V S **P H** K 1 71 0 57 88	(30P, 35P, 36H)	1.2 ± 0.43	0.82 ± 0.22	1.6 ± 0.2	1.2 ± 0.3
38–48	1,087.6	**L** A **C** A I V N T A G R 28 0.1	40C	14.3 ± 1.6	15.1 ± 1.3	28.0 ± 2.0	≫[d]
49–63	1,757.8	E T G G V **H W M** A **F** A **W** N **P R** 4 28 0 0 0 6	60W	2.5 ± 0.2	5.2 ± 0.4	16.0 ± 0.7	13.1 ± 0.6
82–93	1,573.8	Q V **Y** Q **F** E **Y** E S **L L** R 23 2.9 12 4 28	86F	1.2 ± 0.18	0.09 ± 0.02	1.56 ± 0.08	0.07 ± 0.01
95–103	902.4	S A I A S S **P** D R 85	101P	0.35 ± 0.07	0	0.8 ± 0.06	0
104–109	705.4	**C** I T **L** E K 74 35	(104C, 107L)	30.7 ± 3.4	7.8 ± 1.4	4.25 ± 0.4	–
170–180	1,425.7	N Q E Q **L Y** S **F L** E R 0 22 3 0	175Y	0.45 ± 0.04	0	0.59 ± 0.02	0
181–186	805.4	**H** S **P Y F** R 64 73 59 0	183P	0.48 ± 0.09	0	0.9 ± 0.06	0

[a] Rates are derived from data such as that shown in Fig. 2.

[b] The potentially modifiable amino acids are shown in bold with calculated accessible surface area printed below for the free AVP structure (see "Experimental Procedures").

[c] The probe residues indicated by MS/MS spectra for free AVP. The residues that are not confirmed by MS/MS are shown within parentheses. They are likely to be the probe residues, having accessible surface area greater than 20 Å. These peptides are not detected.

[d] More than 50% oxidized peptide was found without any exposure to the x-ray beam.

crystal structure (11). The surface areas (in Å^2) are shown in Table I as numbers below the one-letter amino acid codes for the various tryptic peptides. The solvent accessibilities of individual residues in AVP in the absence of cofactor were also determined from the crystal structure of the binary complex after deleting the pVIc coordinates from the Protein Data Bank (PDB) file (1AVP). The program GETAREA 1.1 (www.scsb.utmb.edu/cgi-bin/get_a_form.tcl) was used to calculate the solvent accessible surface area per residue from the PDB files (24).

Sequence Alignments—AVP protein sequences were retrieved from the National Center for Biotechnology Information Entrez protein sequence database using a Basic Local Alignment Search Tool against the Human Adenovirus type 2 AVP sequence (25). The sequences selected had e-values of $\leq 10^{-60}$ and duplicated sequences were eliminated manually. A total of 26 sequences were chosen for subsequent multiple alignment with the program ClustalW (26) from the European Bioinformatics Institute ClustalW Web server (www.ebi.ac.uk/clustalw) using default parameters. The AVP precursor sequences were also retrieved and aligned, and then C-terminal pVIc peptide sequences were obtained and aligned. Conserved AVP and pVIc sequences were calculated from those alignments and visualized using WebLogo (27) Web server (weblogo.berkeley.edu/) and are shown in Supplementary Fig. 1.

Model Building—The model for the AVP-pVIc-DNA ternary complex was built in O (28), using the PDB coordinates of a 12-mer single-strand AACCGTGCCTCA taken from the structure of a duplex DNA combined with the 1AVP coordinates (11). All the P-O5′ (α) and O3′-P (ϵ) torsion angles (30), most of the O5′-C5′ (β) torsion angles, and several C5′-C4′ (γ) and C3′-O3′ torsion angles were rotated to locate the DNA backbone near the predicted DNA binding regions as well as to adjust the rise per residue to a nearly maximally stretched configuration. Refinements were carried out to optimize the stereochemical parameters in the DNA backbone, using the standard O refinement library. Rotational isomers were evaluated for some of the basic side chain residues (those with high B factors in the crystallographic data) in the vicinity of the DNA binding region to bring them closer to the DNA phosphate groups as well to carbonyl groups in the bases. The coordinates of this model are available at www.aecom.yu.edu/home/csb.

RESULTS

Hydroxyl Radical-mediated Protein Footprinting—AVP and AVP-DNA complexes were exposed to white synchrotron x-ray radiation for periods of 0–150 ms followed by digestion with proteases and separation of the fragments by reverse-phase LC. ESI-MS analysis of the resolved fragments allowed each to be specifically identified. The relative abundances of unmodified and modified peptide ions were calculated from the corresponding peak ion intensities as a function of time of exposure to the synchrotron x-ray beam (12, 22, 23). The fraction of unmodified peptide used in the "dose response" (1 − (modified peptide/(modified + unmodified))) was consistently calculated at all exposure times for free AVP as well as for its complexes. The dose-response curves are presented as unmodified fraction and plotted on a semilogarithmic scale *versus* exposure time. Representative data for tryptic peptides 82–93 and 49–63 derived from free AVP, its two binary complexes, and the ternary complex are shown in Fig. 2. Because of the constant concentration of hydroxyl radicals in the sample during exposure (12, 21–23), the modification reactions followed pseudo first-order kinetics; kinetic fits are shown as solid or dashed lines in Fig. 2. The use of the loss of unmodified fraction as the dependent variable and the con-

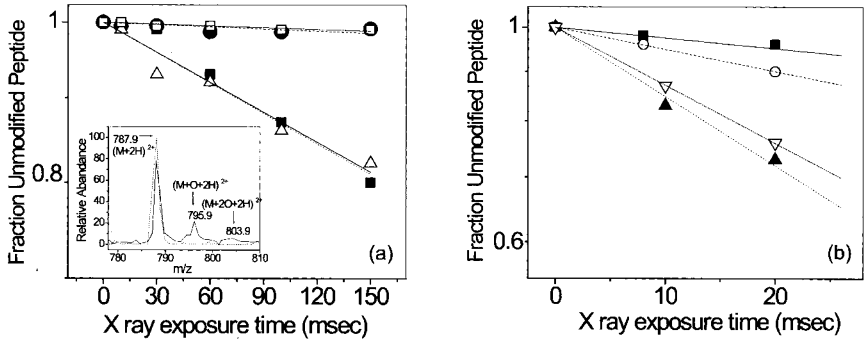

FIG. 2. **Dose-response profiles for the radiolytic modification of tryptic peptide 82–93 derived from free AVP (*solid squares*), AVP-DNA (*solid circles*), AVP-pVIc (*open triangles*), and AVP-pVIc-DNA (*open squares*).** *a*, inset shows the ESI-MS spectra for the same tryptic peptide (MW 1573.8D) in the absence (*solid line*) and in the presence (*dashed line*) of DNA. The exposure time for the inset data was 150 ms. The $(M+2H)^{2+}$ unmodified ion appeared at *m/z* of 787.9, while singly and doubly oxygenated ions appeared at *m/z* values of 795.9 and *m/z* values of 803.9. *b*, dose-response profiles for the radiolytic modification of tryptic peptide 49–63 derived from free AVP (*solid squares*), AVP-DNA (*open circles*), AVP-pVIc (*solid triangles*), and AVP-pVIc-DNA (*open triangles*). The rates of radiolytic modification for these peptides are listed in Table I.

sistent adherence to first order behavior observed in the data indicated that the intact material was probed and that the radiolysis experiments report biologically relevant information. The rate constants for modification for all identified tryptic peptides of free AVP and its complexes with cofactors are listed in Table I.

Peptide 82–93 in free AVP had a modification rate of 1.2 s^{-1} (Fig. 2). Upon binding to DNA, the modification rate decreased over 90% to 0.09 s^{-1}. Binding of pVIc slightly increased the modification rate, while in the ternary complex, as for the binary complex with DNA, the modification rate was reduced over 90%. Protections of this magnitude typically indicate the formation of a buried interface (12–14, 30). The inset to Fig. 2*a* shows the abundance of unoxidized and oxidized peptides in free AVP and the AVP-DNA complex as analyzed by the total ion current signal for a 100 ms exposure. The singly and doubly modified peptides were detected as doubly charged ions at 795.9 *m/z* and 803.9 *m/z*, respectively. Quantitation of the relative abundance of the peaks for the modified and unmodified peptides gave an extent of modified peptide of 20% in the absence of DNA, while in presence of DNA the extent of oxidation for the peptide was only 2%, at an exposure time of 100 ms.

For tryptic peptide 49–63 (Fig. 2*b*), the rate of modification in free AVP was 2.5 s^{-1}; when AVP binds DNA, the modification rate increased 2-fold, while it increased over 6-fold upon binding to pVIc (Fig. 2*b*, Table I). The rate of modification for the ternary complex was slightly less than for the AVP/pVIc binary complex but still increased over 5-fold compared with free AVP. The effects of pVIc binding on the solvent accessibility of probe residues in this region were striking, because the pVIc cofactor binds on the opposite side of D1 to peptide 49–63, which is within S2 and the loop between S2 and S3 (Fig. 1*a*). These data indicated allosteric communication between the cofactor binding site and the active site; such allosteric effects have been frequently observed in protein footprinting experiments (14–17, 31).

Analyzing the dose-response curves for the other tryptic peptides as well as chymotryptic peptides obtained from free AVP, AVP-DNA, AVP-pVIc, and AVP-pVIc-DNA molecule illustrates the significant changes in the rate of modification (both increases and decreases) upon cofactor binding to the AVP molecule for many peptides (Table I, Supplemental Table I, Fig. 3). The modification rate data for all nine tryptic peptides of AVP and the AVP-pVIc-DNA ternary complex as well as that for six chymotryptic peptides are shown in bar graph format in Fig. 3.

N-terminal Segments of AVP—In free AVP, the N-terminal tryptic peptide (residues 1–9) had a modification rate of 11.2 s^{-1}, consistent with the peptide containing a highly accessible methionine residue (Table I). There was over a 90% decrease in reactivity for this peptide upon DNA binding in either the binary or ternary complex. Due to poor MS signals for peptide 1–9 in the AVP-pVIc binary complex, we were unable to determine its rate of modification. Chymotryptic peptide 16–21 (GCGPYF) showed no change in its modification rate on cofactor binding and a low rate of modification overall from ~0.5–0.6 s^{-1} (Fig. 3), indicating that the probe residues in this segment were relatively buried and that they did not become more or less exposed upon AVP binding to its cofactors. Tryptic peptide 29–37 showed no change (within error) in its modification rate when free AVP was compared with its binary and ternary complexes (Table I, Fig. 3).

Allosteric Effects of Cofactor Binding in the Active Site Cleft—Tryptic peptide 38–48 had a very large modification rate in free AVP that is not consistent with the calculated surface area of Leu^{38} or Cys^{40}. LC-coupled MS analysis showed considerable abundance of doubly oxidized peptide (560.8 *m/z*) at short exposure times relative to that of singly oxidized peptide (552.8 *m/z*). This indicated the oxidation of Cys^{40} in the peptide; tandem MS analysis (data not shown) confirmed Cys^{40} as the probe residue in free AVP. The rate of

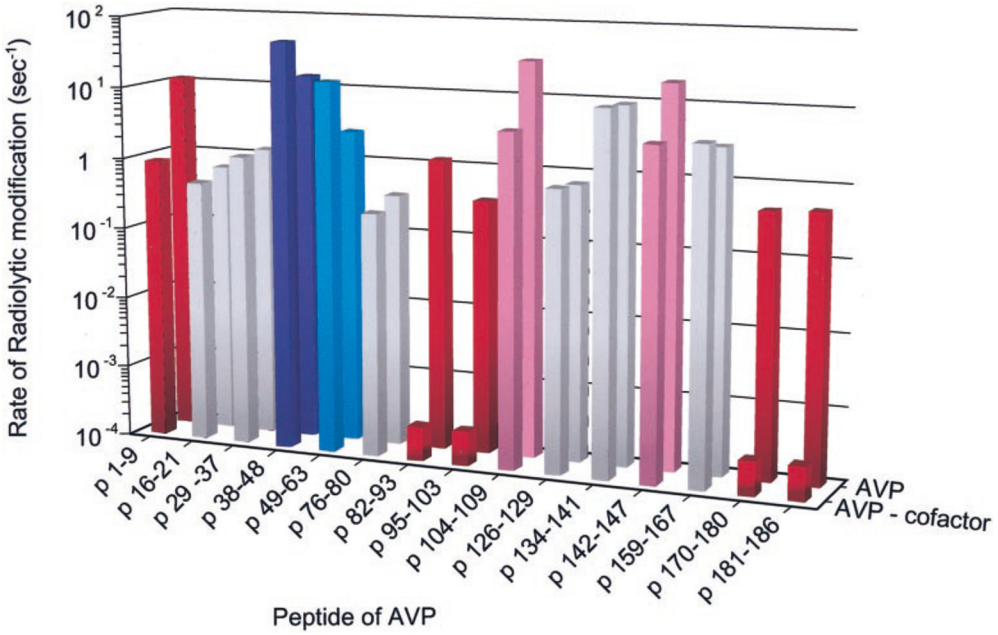

FIG. 3. **Bar graph showing the rate of modification of the tryptic and chymotryptic peptides obtained from free AVP (*back row*) and of AVP-pVIc-DNA (*front row*).** Because data for the ternary complex of peptide 104–109 and 142–147 were not available, data for the AVP-pVIc complex is shown instead for these peptides. *Red* in the figure indicates a DNA-dependent protection; *blue* indicates enhancement of reactivity due to cofactor binding (see Table I); *pink* indicates pVIc-dependent protections; and *gray* indicates no observed change in reactivity. The identical color scheme is used in Fig. 4.

modification increased 2-fold on binding pVIc, while it was unchanged upon binding to DNA, indicating that Cys^{40} became more reactive due to allosteric effects of peptide binding. Calculation of the rate of modification for the ternary complex was difficult due to the existence of a very large level of background oxidation for Cys^{40} at zero exposure time. LC-ESI-MS analysis showed free AVP had $<1\%$ of oxidized Cys^{40} at 0 ms exposure time. However, for the AVP-DNA-pVIc complex, $>50\%$ Cys^{40} was found to be oxidized without any exposure to x-rays. The chemical reactivity of Cys^{40} was higher than would be expected from its predicted buried surface area, and it was significantly increased by peptide binding. Its reactivity to air oxidation in the ternary complex was extraordinary.

Peptide 49–63, like peptide 38–48, became more reactive upon peptide binding but it also became more reactive upon binding DNA. These results were indicative of allosteric effects upon binding of either cofactor. Tandem MS was carried out to identify the site(s) of oxidation for peptide 49–63 (ETGGVHWMAFAWNPR) to specifically identify the probe residue experiencing conformational changes. In tandem experiments a specific peptide fragment is selected by the first stage of the mass spectrometer for CID in the second stage (see Supplemental Fig. 2). The masses of the generated fragment peptides were measured and the site of fragmentation was determined by the observed masses of the fragments. When an oxidized fragment is selected in the first stage and fragmented, the fragments that retain the mass shift are indicated to contain the original probe residue. For peptide 49–63, MS/MS indicated that potential probes Trp^{55} or Met^{56} were not oxidized in free AVP; the modified residue in free AVP was Trp^{60} because a $y_4+16\text{-}NH_3$ ion with minimal y_4 was observed and b_8 was seen to be predominantly unmodified (SF2). MS/MS analysis of same peptide in the ternary complex had a similar pattern, with the exception that a b_9+16 ion was observed, indicating that Trp^{55} or Met^{56}, in addition to Trp^{60}, was oxidized upon cofactor binding. Thus, the former residues became more solvent-accessible upon cofactor binding.

Peptides Protected on DNA Binding—Peptide 82–93 (QVYQFEYESLLR) has multiple residues that could possibly give rise to oxidation (Table I). MS/MS sequencing was carried out on free AVP and its complex to determine the oxidation site(s) (data not shown). The y-type ions identified supported Phe^{86} as the primary oxidation site. The rate of modification of 1.2 s^{-1} thus corresponded to the oxidation of a slightly solvent accessible Phe^{86} residue, which is almost entirely buried upon DNA binding. For tryptic peptide 95–103, virtually 100% protection was observed upon DNA binding in the binary or ternary complex, while pVIc binding increased the modification rate about 2-fold. Thus, this peptide was located at a site of potential DNA binding as well as a site of allosteric conformational change induced by peptide binding. MS/MS data clearly identifies Pro^{101} as the probe residue (data not shown). Within peptide 104–109, Cys^{104} forms a disulfide bond with the pVIc cofactor. The rate of modification of this peptide in free AVP was large (30.7 s^{-1}), consistent

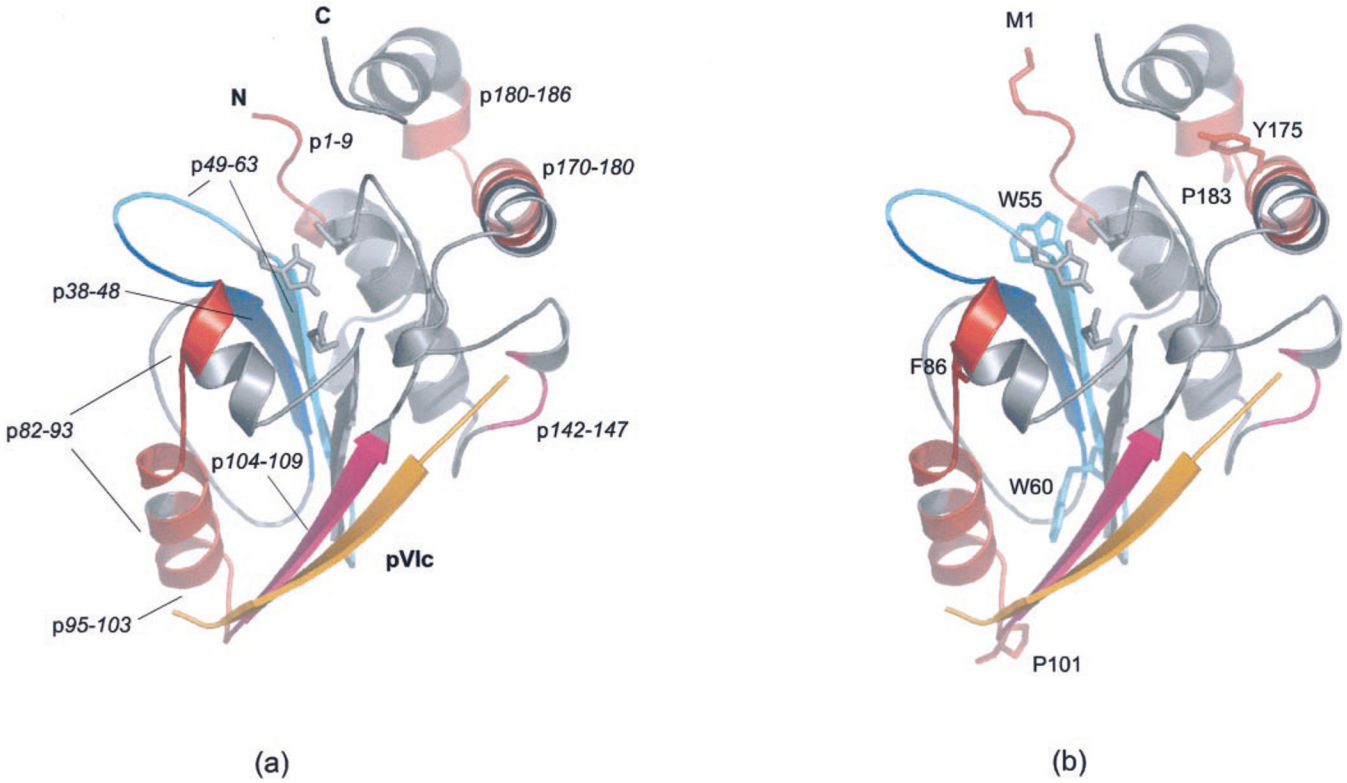

FIG. 4. **Ribbon diagram representation of the AVP-pVIc complex.** pVIc is shown in *orange*. *a*, the peptides that showed a decrease in modification rate due to DNA (or pVIc) binding are shown in *red* (*pink*). The peptides that showed an increase in modification rate due to cofactor binding are shown in *blue* (see Table I). *b*, ribbon diagram of AVP structure in the same orientation as *a*, with the side chain probes residues identified by MS/MS indicated.

with the high solvent accessibility of Cys^{104} (74 $Å^2$) and Leu^{107} (35 $Å^2$) in the absence of peptide. Upon pVIc binding, Cys^{104} and Leu^{107} become protected, with solvent accessible surface areas reduced to 15 and 1 $Å^2$, respectively, while the rate of modification was reduced by ~85%. In addition, DNA binding showed a ~75% protection of this peptide. Unfortunately, tandem MS data could not be obtained for this peptide; however, Cys^{104} and Leu^{107} represent the likely probe sites.

C-terminal Peptide Interactions with Peptide and DNA Cofactors—Chymotryptic peptide 142–147 showed a significant decrease in the rate of modification on pVIc binding (Fig. 3, ST1). Protection of peptide 142–147 is consistent with the x-ray structure where Met^{147} is seen to interact with the N terminus of the pVIc peptide (Fig. 1*a*). Two peptides near the N terminus of AVP in D2 detected by MS were tryptic peptides 170–180 and 181–186. These peptides showed similar trends in their modification rates compared with peptides 82–93 and 95–103. Peptides 170–180 and 181–186 showed virtually 100% protection from modification when DNA was bound but experienced no changes in modification rate upon pVIc binding alone. These results are consistent with burial of their probe residues upon DNA binding. For peptide 170–180, MS/MS analysis of doubly charged, singly oxidized peptide indicated Tyr^{175} as the probe site, while for peptide 181–186, tandem data indicated Pro^{183} was the primary probe residue.

DISCUSSION

AVP contains two domains (D1 and D2) with the active site located in a cleft formed by the interacting surfaces of the subdomains (Fig. 1*a*). Active site residues His^{54}, Glu^{71}, and Cys^{122}, which are located deep within this cleft, are entirely conserved in a multiple alignment analysis of 26 sequences using ClustalW (Glu^{71} can be an Asp residue, SF1). The positions of these three residues in AVP can be superimposed on the active site of the archetypical cysteine proteinase papain, and this has led to the hypothesis that AVP and papain utilize a similar catalytic mechanism (7, 11, 32–34). His^{54} and Cys^{122}, the active site nucleophile of AVP, which may form an ion pair, are located on opposite subdomains. Thus, the enzyme's activity is dependent on the relative positioning of the two domains. The bound pVIc cofactor bridges the subdomains; thus, the molecular mechanism by which it activates AVP may involve reorienting the subdomain interface.

pVIc-AVP Binding—The interactions of AVP and pVIc are well understood from the 1.6 Å resolution crystal structure of AVP-pVIc complex and include hydrogen bonds, ion pair interactions, van der Waals interactions, and a disulfide bond (5–7, 11). The solution footprinting data is entirely consistent with these crystallographic predictions, as peptide 104–109, which contains the disulfide bonded Cys^{104} as well as Leu^{107},

experiences a 4-fold decrease in reactivity upon pVIc binding to AVP, consistent with the significant reductions in solvent accessibility predicted from the crystallographic data (Table I, Fig. 4, *a* and *b*). Cys^{104} is absolutely conserved in all known AVP sequences while Leu^{107} is preferred. Within peptide 142–147, the highly conserved Met^{147} in domain D2 forms an interdomain hydrogen bond with the entirely conserved $Gly^{1'}$ at the N terminus of pVIc. This peptide also experiences a protection in the AVP-pVIc binary complex consistent with this interaction. This protection is shown in Fig. 4, *a* and *b*. In Fig. 4*a*, the peptides exhibiting DNA-dependent protections are colored in red, while the pVIc-dependent protections are colored pink. Peptides exhibiting DNA- or pVIc-dependent enhancements in reactivity are colored in blue. Fig. 4*b* illustrates the probe residues for each of these peptides.

Cofactor-induced Conformational Changes—Biochemical studies show that the two cofactors, pVIc and DNA increase the k_{cat} for substrate hydrolysis and decrease the K_m (8). The k_{cat} for AVP increases by 117-fold due to the presence of pVIc, whereas the K_m decreases 10-fold. For DNA binding to AVP, the effect on k_{cat} and K_m is about equal, with an 11-fold increase and a 10-fold decrease, respectively. The increased rates of modification for peptides 38–48 and 49–63 upon cofactor binding indicated increased "spatial" availability of the cleft to substrates as well as changes in the chemical reactivity of residues within the cleft. The reactivity of peptide 38–48 was not influenced by DNA binding alone but exhibited a 2-fold increased reactivity upon binding pVIc (Fig. 4, *a* and *b*). However, in the ternary complex, Cys^{40} was extraordinarily sensitive to oxidation, even by air. Within peptide 38–48, Thr-45 is predicted to be hydrogen bonded to His^{54}, which has a relationship to Cys^{122} similar to that seen in papain; the negatively charged Cys^{122} is ion paired to protonated His^{54}, generating a very active nucleophilic species (33, 34). As the k_{cat} of the enzyme is increased nearly ~1,300-fold by the binding of both cofactors, it may be the case that the Cys^{122} ion pair is not formed until one or both cofactors bind enzyme. The extraordinary changes in reactivity of Cys^{40} imply that it may be involved (or sensitive to) the charge relay network that promotes ion-pair formation in the ternary complex.

Peptide 49–63, like 38–48, lines the interdomain active site cleft. Unlike peptide 38–48, its reactivity increased upon either DNA binding (2-fold) or pVIc binding alone (6-fold). For free AVP, Trp^{60} was the sole probe residue, while in the ternary complex, Trp^{55} and Met^{66}, which are within 5 Å of the active site His^{54} and Cys^{122} residues, became more solvent accessible and were oxidized. Trp^{60} and Trp^{55} are conserved, primarily to preserve the architecture of the binding pocket. These data provide convincing evidence that cofactor binding to AVP changed the structure at the active site. In the case of pVIc binding, a possible molecular explanation for this reactivity change includes subdomain rearrangements mediated by interactions of the pVIc peptide across the interface between domains 1 and 2 (Fig. 1*a*). This raises the question as to the molecular mechanisms by which DNA binding provides a similar activation, as well as how the two cofactors work together to provide maximal activity for the enzyme.

Nonspecific Binding of DNA to AVP—The surface charges of AVP are shown in Fig. 1*b* (11); a number of positively charged surface patches are indicated in blue that could be potential interaction sites with the negatively charged DNA backbone. Many examples of sequence-specific interactions of DNA with DNA-binding proteins are known (35–39); fewer examples illustrate the nature of nonspecific recognition of ssDNA by proteins (40–45). In general, many DNA-protein interactions are in part mediated by long-range columbic interactions that bring the DNA into close proximity to the protein forming a "loose" dynamic complex (40). After this nonspecific binding, which is well precedented in the case of restriction enzymes (46), specific binding then can occur at the cognate site mediated by the formation of charge-charge interactions, specific hydrogen bonding, van der Walls contacts, and base stacking interactions (35–37, 40, 45, 47). The footprinting data clearly indicated DNA-dependent protections for five peptides (Fig. 4, *a* and *b*), where the extent of protection (>90%) was consistent with burial of the respective probe sites in a macromolecular interface (12–14, 30). However, ligand-induced reorganization of structure may also contribute to burial of these residues (15–17, 31). The buried probe residues are indicated in Fig. 4*b* and include Met^{1}, Pro^{183}, and Tyr^{175} in D2, which are located on the opposite side of the molecule to Phe^{86} and Pro^{101} in D1. Because the stoichiometry of DNA-AVP binding is 1:1 for the 12-mer ssDNA used here (8), we considered the possibility that the DNA could be stretched across the AVP molecule so as to bury residues within both D1 and D2.

Detailed Model of DNA-AVP Interactions—The DNA-AVP interface was modeled using a 12-mer ssDNA with the sequence GACGACTAGGAT. The constraints in the modeling included DNA-dependent protection of the above probe residues, satisfaction of potential favorable charge or base stacking interactions, use of conserved residues to provide the trace of the DNA-AVP interaction, and reasonable constraints on the bond lengths and angles of the macromolecules. The final model (Fig. 5, *a* and *b*) satisfies many of these constraints, in particular solvent accessibility calculations; the coordinates of the ternary complex compared with that of the AVP-pVIc binary complex showed DNA-dependent protections from solvent for Phe^{86}, Pro^{101}, Pro^{183}, and Tyr^{175}.

In domain D1, the well-conserved, basic amino acid residues Lys^{81} on H2, Arg^{93} on H3, and Arg^{103} on S5 from AVP and $Lys^{6'}$, $Arg^{7'}$, $Arg^{8'}$, and $Arg^{9'}$ from pVIc provide charge interactions with the DNA. DNA binds to AVP much more tightly when pVIc is bound, suggesting specific interactions between cofactor peptide and DNA. Such interactions and the binding of DNA in this region (as predicted by the model) can be indirectly supported by the footprinting analysis of peptide 104–109. In absence of pVIc, this peptide was 4-fold pro-

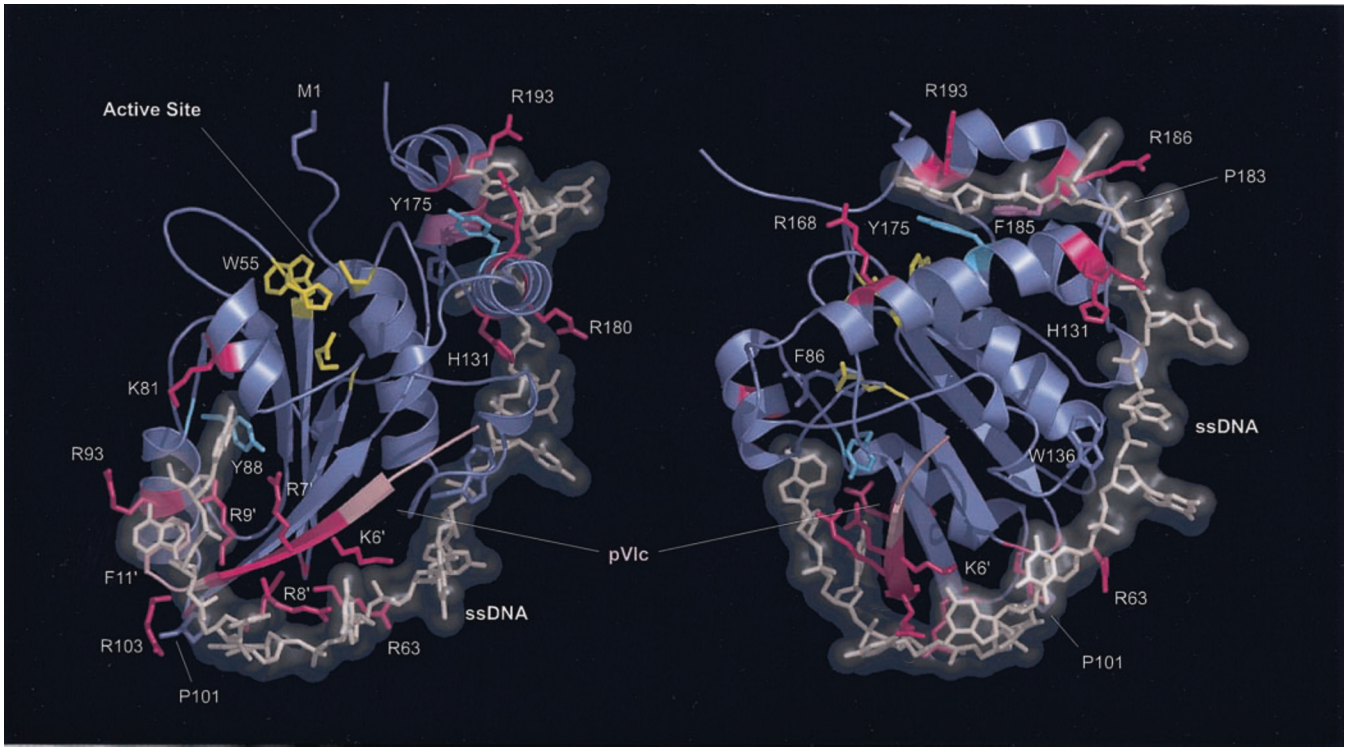

FIG. 5. **A model for DNA binding to AVP-pVIc complex is shown in two different orientations.** The AVP-pVIc complex is shown in ribbon format, where AVP and pVIc are colored in *slate* and *light pink*, respectively. The ssDNA has a stick representation and is colored *off-white*. The amino acid residues proposed to interact with DNA are represented with *dark pink* for basic (Arg, His, and Lys), *cyan* for Tyr, *magenta* for Phe from AVP, and *light pink* for Phe from pVIc. The probe residues identified by MS/MS are also indicated and highlighted with the same colors of the AVP ribbon diagram. The active site residues and Trp-55 are also colored *yellow*.

tected upon DNA binding, strongly indicating that DNA binds to this segment of free AVP. DNA binding to D1 can be further stabilized by base stacking interactions with the solvent-exposed, highly conserved Tyr^{88} near the beginning of H3 in AVP and $Phe^{11'}$ from pVIc (Fig. 5*a*). The model does not predict specific interactions with Phe^{86} on the loop connecting H2 and H3; however, the model predicts a significant reduction of solvent accessibility for this residue upon DNA binding consistent with the observed DNA-dependent protection (Table I).

In domain D2, residues Arg^{168} and Arg^{180} that span H5, His^{181} found between H5 and H6, Arg^{186} on H6, and Arg^{193} on H7 provide ionic interactions with DNA as well as H-bonding interactions. Of these residues, Arg^{193} is strongly conserved, but the vast majority of substitutions for all these residues are charged or polar. DNA binding to domain 2 can be stabilized by base stacking with surface-exposed Tyr^{175} on H5 within a hydrophobic cleft created by Tyr^{175} and Phe^{185}; these two residues are entirely conserved. Additional interactions that can further stabilize the DNA can be mediated through Arg^{63} and Lys^{65} in domain D1 and His^{131} and Trp^{136} in the loop joining H4 and S6 in domain D2. Because no DNA-dependent protections were observed in these regions, binding to these residues may be dominated by water-mediated hydrogen-bonding interactions (41). The model does not directly explain the DNA-dependent protection of Met^{1}; DNA-dependent subunit reorientation may induce an allosteric change that results in protection of this residue.

Although this model of DNA binding was constructed based on predicted interactions with a 12-mer ssDNA, we suggest that it provides a general model of AVP-DNA binding. AVP binds longer single-stranded sequences than a 12-mer and, *in vivo*, binds to double-stranded DNA. The model predicts a significant bending of the ssDNA, which is obviously quite flexible. However, bending of double-stranded DNA in the process of protein binding is well precedented. The co-crystal structure of Integration Host Factor bound to its specific binding site (the so-called H' site) shows the DNA wrapped around the protein in a U-turn that exceeds 180° (48). TATA-binding protein (TBP) binding to DNA also induces kinks in the DNA sequence where the TATA box sequences interact with the concave surface of TBP by bending toward the major groove, producing a wide open minor groove. Phenylalanine residues from TBP provide specific base-stacking interactions with the DNA (49–51). Based on these considerations, it is reasonable that the combination of conserved positively charged patches on AVP and its conserved aromatic residues that are poised for base-stacking interactions provides a facile surface for binding and bending double-stranded DNA. Thus, our model provides an overall framework for predicting

AVP-DNA interactions and suggests that DNA binding provides a molecular strap reorienting the positions of the two subdomains directly influencing the reactivity of the active site. In addition, both pVIc and DNA may independently provide this reorientation as well as drive it cooperatively to fully activate AVP.

CONCLUSIONS

Synchrotron protein footprinting was used to determine the structural changes within AVP upon formation of complexes with its activating cofactors. The data revealed cofactor-dependent conformational changes at the catalytic site related to functional activation. Footprinting data of the binary complex of AVP with DNA as well as the ternary complex of AVP and both of its cofactors revealed potential sites of DNA contact with AVP on both domains of the molecule adjacent to conserved patches of positive charge. A molecular model of the AVP-DNA-pVIc ternary complex is proposed that is consistent with the footprinting data and the observed sequence conservation, as well as providing a molecular mechanism of activation that explains the synergistic effects of the two cofactors.

Acknowledgments—We thank M. L. Baniecki for assistance in some of the preliminary experiments.

* This research is supported in part by The Biomedical Technology Centers Program of the National Institute for Biomedical Imaging and Bioengineering (P41-EB-01979, M. R. C.), the Innovative Molecular Analysis Technologies Program of the National Cancer Institute (R33-CA-83179, M. R. C.), the Office of Biological and Environmental Research of the U.S. Department of Energy under Prime Contract DE-AC0298CH10886 with Brookhaven National Laboratory (W. F. M.), and by National Institutes of Health Grant AI41599 (W. F. M.). J. L. P. and D. W. L. were supported by the Department of Energy's Office of Science by Science Undergraduate Laboratory Internships. The National Synchrotron Light Source is supported by the Department of Energy, Division of Materials Sciences.The costs of publication of this article were defrayed in part by the payment of page charges. This article must therefore be hereby marked "*advertisement*" in accordance with 18 U.S.C. Section 1734 solely to indicate this fact.

[S] The on-line version of this manuscript (available at http://www.mcponline.org) contains supplemental material.

¶ To whom correspondence should be addressed: Center for Synchrotron Biosciences, Department of Physiology & Biophysics, Albert Einstein College of Medicine, Bronx, NY. 10461. Tel.: 718-430-4136; Fax: 718-430-8587; E-mail: mrc@aecom.yu.edu.

REFERENCES

1. Weber, J. M., and Anderson, C. W. (1988) Identification of the gene coding for the precursor of adenovirus core protein X. *J. Virol.* **62,** 1741–1745
2. Weber, J. (1976) Genetic analysis of adenovirus type 2 III. Temperature sensitivity of processing viral proteins. *J. Virol.* **17,** 462–471
3. Webster, A., and Kemp, G. (1993) The active adenovirus protease is the intact L3 23K protein. *J. Gen. Virol.* **74,** 1415–1420
4. Webster, A., Hay, R. T., and Kemp, G. (1993) The adenovirus protease is activated by a virus-coded disulphide-linked peptide. *Cell* **72,** 97–104
5. Mangel, W. F., McGrath, W. J., Toledo, D. L., and Anderson, C. W. (1993) Viral DNA and a viral peptide can act as cofactors of adenovirus virion proteinase activity. *Nature* **361,** 274–275
6. Baniecki, M. L., McGrath, W. J., McWhirter, S. M., Li, C., Toledo, D. L., Pellicena, P., Barnard, D. L., Thorn, K. S., and Mangel, W. F. (2001) Interaction of the human adenovirus proteinase with its 11-amino acid cofactor pVIc. *Biochemistry* **40,** 12349–12356
7. McGrath, W. J., Ding, J., Didwania, A., Sweet, R. M., and Mangel, W. F. (2003) Crystallographic structure at 1.6-A resolution of the human adenovirus proteinase in a covalent complex with its 11-amino-acid peptide cofactor: insights on a new fold. *Biochim. Biophys. Acta* **1648**, 1–11
8. McGrath, W. J., Baniecki, M. L., Li, C., McWhirter, S. M., Brown, M. T., Toledo, D. L., and Mangel, W. F. (2001) Human adenovirus proteinase: DNA binding and stimulation of proteinase activity by DNA. *Biochemistry* **40,** 13237–13245
9. McGrath, W. J., Baniecki, M. L., Peters, E., Green, D. T., and Mangel, W. F. (2001) Roles of two conserved cysteine residues in the activation of human adenovirus proteinase. *Biochemistry* **40,** 14468–14474
10. Rancourt, C., Keyvani-Amineh, H., Sircar, S., Labrecque, P., and Weber, J. M. (1995) Proline 137 is critical for adenovirus protease encapsidation and activation but not enzyme activity. *Virology* **209,** 167–173
11. Ding, J., McGrath, W. J., Sweet, R. M., and Mangel, W. F. (1996) Crystal structure of the human adenovirus proteinase with its 11 amino acid cofactor. *EMBO J*. **15,** 1778–1783
12. Guan, J. Q., Vorobiev, S., Almo, S C., and Chance, M. R. (2002) Mapping the G-actin binding surface of cofilin using synchrotron protein footprinting. *Biochemistry* **41,** 5765–5775
13. Rashidzadeh, H., Khrapunov, S., Chance, M. R., and Brenowitz, M. (2003) Solution structure and interdomain interactions of the Saccharomyces cerevisiae "TATA Binding Protein" (TBP) probed by radiolytic protein footprinting. *Biochemistry* **42,** 3655–3665
14. Liu, R., Guan, J. Q., Zak, O., Aisen, P., and Chance, M. R. (2003) Structural reorganization of transferrin C-lobe and transferrin receptor upon complex formation: C-lobe to the receptor helical domain. *Biochemistry* **42**, 12447–12454
15. Guan, J.G., Almo, S. C., Reisler, E., and Chance, M. R. (2003) Structural reorganization of proteins revealed by radiolysis and mass spectrometry: G-actin solution structure is divalent cation dependent. *Biochemistry* **42**, 11992–12000
16. Kiselar, J. G., Janmey, P. A., Almo, S. C., and Chance, M. R. (2003) Visualizing the Ca^{2+}-dependent activation of gelsolin by using synchrotron footprinting. *Proc. Natl. Acad. Sci. U. S. A.* **100,** 3942–3947
17. Kiselar, J. G., Janmey, P. A., Almo, S. C., and Chance, M. R. (2003) Structural analysis of gelsolin using synchrotron protein footprinting. *Mol. Cell. Proteomics* **2,** 1120–1132
18. Mangel, W. F., Toledo, D. L., Brown, M. T., Martin, J. H., and McGrath, W. J. (1996) Characterization of three components of human adenovirus proteinase activity *in vitro*. *J. Biol. Chem.* **271,** 536–543
19. Jensen, D. E., Kelly, R. C., and von Hippel, P. H. (1976) DNA "melting" proteins. II. Effects of bacteriophage T4 gene 32-protein binding on the conformation and stability of nucleic acid structures. *J. Biol. Chem.* **251,** 7215–7228
20. Pace, C. N., Vajdos, F., Fee, L., Grimsley, G., and Gray T. (1995) How to measure and predict the molar absorption coefficient of a protein. *Protein Sci.* **4,** 2411–2423
21. Ralston, C. Y., Sclavi, B., Sullivan, M., Deras, M. L., Woodson, S. A., Chance, M. R., and Brenowitz, M. (2000) Time-resolved synchrotron X-ray footprinting and its application to RNA folding. *Methods Enzymol.* **317**, 353–368
22. Maleknia, S. D., Ralston, C. Y., Brenowitz, M. D., Downard, K. M., and Chance, M. R. (2001) Determination of macromolecular folding and structure by synchrotron x-ray radiolysis techniques. *Anal. Biochem.* **289,** 103–115
23. Kiselar, J. G., Maleknia, S. D., Sullivan, M., Downard, K. M., and Chance, M. R. (2002) Hydroxyl radical probe of protein surfaces using synchrotron X-ray radiolysis and mass spectrometry. *Int. J. Radiat. Biol.* **78,** 101–114
24. Fraczkiewicz, R., and Braun, W. (1998) Exact and efficient analytical calculation of the accessible surface areas and their gradients for macromolecules. *J. Comput. Chem.* **19,** 319–333
25. Altschul, S. F., Madden, T. L., Schaffer, A. A., Zhang, J., Zhang, Z., Miller, W., and Lipman, D. J. (1997) Gapped BLAST and PSI-BLAST: A new generation of protein database search programs. *Nucleic Acids Res.* **25,** 3389–3402
26. Thompson, J. D., Higgins, D. G., and Gibson, T. J. (1994) CLUSTAL W:

Improving the sensitivity of progressive multiple sequence alignment through sequence weighting, position-specific gap penalties and weight matrix choice. *Nucleic Acids Res.* **22,** 4673–4680
27. Crooks, G., Hon, G., Chandonia, J. M., and Brenner S. E. (2004) Weblogo: A sequence logo generator. *Genome Res.* **14,** 1188–1190
28. Jones, T. A., Zou, J. Y., Cowan, S. W., and Kjeldgaard, M. (1991) Improved methods for building protein models in electron density maps and the location of errors in these models. *Acta Crystallogr. A* **47,** 110–119
29. Saenger, W. (1984) *Principles of Nucleic Acid Structure*, Springer-Verlag, New York
30. Goldsmith, S. C., Guan, J. Q., Almo, S., and Chance, M. (2001) Synchrotron protein footprinting: A technique to investigate protein-protein interactions. *J. Biomol. Struct. Dyn.* **19,** 405–418
31. Guan, J. Q., Almo, S., and Chance, M. R. (2004) Synchrotron Radiolysis and Mass Spectrometry: A new approach to research on the actin cytoskeleton. *Acc. Chem. Res.* **37,** 221–229
32. Harrison, M. J., Burton, N. A., and Hillier, I. H. (1997) Catalytic mechanism of the enzyme papain: Predictions with a hybrid quantum mechanical/molecular mechanical potential. *J. Am. Chem. Soc.* **119,** 12285–12291
33. Storer, A. C., and Menard, R. (1994) Catalytic mechanism in papain family of cysteine peptidases. *Methods Enzymol.* **244,** 486–500
34. Barbezange, C., Benko, M., Dan, A., and Harrach, B. (2000) DNA sequencing and phylogenetic analysis of the protease gene of ovine adenovirus 3 suggest that adenoviruses of sheep belong to two different genera. *Virus Res.* **66,** 79–85
35. Peersen, O. B., Ruggles, J. A., and Schultz, S. C. (2002) Dimeric structure of the Oxytricha nova telomere end-binding protein alpha-subunit bound to ssDNA. *Nat. Struct. Biol.* **9,** 182–187
36. Theobald, D. L., and Schultz, S. C. (2003) Nucleotide shuffling and ssDNA recognition in Oxytricha nova telomere end-binding protein complexes. *EMBO J.* **22,** 4314–4324
37. Kerr, I. D., Wadsworth, R. I., Cubeddu, L., Blankenfeldt, W., Naismith, J. H., White, M. F. (2003) Insights into ssDNA recognition by the OB fold from a structural and thermodynamic study of Sulfolobus SSB protein. *EMBO J.* **22,** 2561–2570
38. Luscombe, N. M., Laskowski, R. A., and Thornton, J. M. (2001) Amino acid-base interactions: A three-dimensional analysis of protein-DNA interactions at an atomic level. *Nucleic Acids Res.* **29,** 2860–2874
39. Jones, S., van Heyningen, P., Bermanm, H. M., and Thornton, J. M. (1999) Protein-DNA interactions: A structural analysis. *J. Mol. Biol.* **287,** 877–896
40. Sun, J., Viadiu, H., Aggarwal, A. K., and Weinstein, H. (2003) Energetic and structural considerations for the mechanism of protein sliding along DNA in the nonspecific BamHI-DNA complex. *Biophys J.* **84,** 317–325
41. Murphy, F. V., IV, and Churchill, M. E. (2000) Nonsequence-specific DNA recognition: A structural perspective. *Structure Fold Des.* **8,** R83–R89
42. Bochkarev, A., Pfuetzner, R. A., Edwards, A. M., and Frappier, L. (1997) Structure of the single-stranded-DNA-binding domain of replication protein A bound to DNA. *Nature* **385,** 176–181
43. Viadiu, H., and Aggarwal, A. K. (2000) Structure of BamHI bound to nonspecific DNA: A model for DNA sliding. *Mol. Cell* **5,** 889–895
44. Allain, F. H., Yen, Y. M., Masse, J. E., Schultze, P., Dieckmann, T., Johnson, R. C., and Feigon, J. (1999) Solution structure of the HMG protein NHP6A and its interaction with DNA reveals the structural determinants for non-sequence-specific binding. *EMBO J.* **18,** 2563–2579
45. Raghunathan, S., Kozlov, A. G., Lohman, T. M., and Waksman, G. (2000) Structure of the DNA binding domain of *E. coli* SSB bound to ssDNA. *Nat. Struct. Biol.* **7,** 648–652
46. Pingoud, A., and Jeltsch, A. (2001) Structure and function of type II restriction endonucleases. *Nucleic Acids Res.* **29,** 3705–3727
47. Anderson, E. M., Halsey, W. A., and Wuttke, D. S. (2003) Site-directed mutagenesis reveals the thermodynamic requirements for single-stranded DNA recognition by the telomere-binding protein Cdc13. *Biochemistry* **42,** 3751–3758
48. Rice, P. A., Yang, S., Mizuuchi, K., and Nash, H. A. (1996) Crystal structure of an IHF-DNA complex: A protein-induced DNA U-turn. *Cell* 87**,** 1295–1306
49. Kim, J. L., Nikolov, D. B., and Burley, S. K. (1993) Co-crystal structure of TBP recognizing the minor groove of a TATA element. *Nature* **365,** 520–527
50. Juo, Z. S., Chiu, T. K., Leiberman, P. M., Baikalov, I., Berk, A. J., and Dickerson, R. E. (1996) How proteins recognize the TATA box. *J. Mol. Biol.* **261,** 239–254
51. Kim, Y., Geiger, J. H., Hahn, S., and Sigler, P. B. (1993) Crystal structure of a yeast TBP/TATA-box complex. *Nature* **365,** 512–520